Food Chemistry 275 (2019) 176–185

Contents lists available at ScienceDirect

Food Chemistry

journal homepage: www.elsevier.com/locate/foodchem

Identification and structural analysis of cereal arabinoxylan-derived oligosaccharides by negative ionization HILIC-MS/MS

Minna Juvonen[a,*], Markus Kotiranta[a], Jouni Jokela[b], Päivi Tuomainen[a], Maija Tenkanen[a]

[a] Department of Food and Nutrition, University of Helsinki, P.O. Box 66, 00014, University of Helsinki, Finland
[b] Department of Microbiology, University of Helsinki, P.O. Box 56, 00014, University of Helsinki, Finland

ARTICLE INFO

Keywords:
Tandem mass spectrometry
Oligosaccharides
Arabinoxylan
Negative ionization
Linkage analysis

ABSTRACT

Recent works provide evidence of the prebiotic potential of arabinoxylan-derived oligosaccharides (A)XOS. In this study, we developed a structural analysis for cereal-derived (A)XOS by negative ionization HILIC-MS/MS. Initially, we assessed twelve (A)XOS samples of known structures with different linkage positions and branching points by direct-infusion negative ESI-MS^n. We subsequently developed the negative ion HILIC-MS/MS with a post-column addition of ammonium chloride. The selected (A)XOS represented both linear (arabinofuranosyl residue linked to the non-reducing end of xylooligosaccharide) and branched structures. Each (A)XOS sample produced a specific spectrum in negative ion ESI-MS^n. By analyzing cross-ring fragment ions, we determined the linkage positions of linear (A)XOS. The presence or absence of diagnostic ions in the MS^3 allowed us to detect different branches (*O*-2- or/and *O*-3-linked arabinofuranosyl with/or without *O*-4-linked xylopyranosyl at the non-reducing end). Furthermore, we could identify all analyzed samples by HILIC-MS/MS, based on the formed spectral library and chromatographic retention times.

1. Introduction

Arabinoxylan (AX) is a major polysaccharide found in the cell walls of cereal grain endosperm (Saulnier, Guillon, Sado, & Rouau, 2007). AX degrades to (arabino)xylooligosaccharides [(A)XOS] by enzymatic hydrolysis in the colon by means of intestinal microbiota or during food processing, such as brewing (Broekaert et al., 2011). Both AX and (A)XOS are considered as dietary fibers (Mendis & Simsek, 2014). (A)XOS include both xylooligosaccharides (XOS) and arabinoxylooligosaccharides (AXOS). Since recent studies have shown evidence of the prebiotic effects of AX and (A)XOS in the colons of humans and animals, interest in them has increased. AX and (A)XOS are associated with many health benefits, including immunomodulatory activity and attenuation of type II diabetes (Mendis & Simsek, 2014). (A)XOS have also been reported to attenuate serum cholesterol, triglyceride, and glucose levels (Broekaert et al., 2011).

Cereal grain AX consists of β(1 → 4)-linked xylopyranosyl residue (Xyl*p*) backbone with arabinose mono- and di-substituents, as reviewed by Biliaderis and Izydorczyk (2007), Izydorczyk and Biliaderis (1995) and Saulnier et al. (2007). Arabinose substituents are α(1 → 2)- or α(1 → 3)-linked furanosyl residues (Ara*f*) or both. Small amounts of β-D-Xyl*p*-(1 → 2)-α-L-Ara*f*-(1 → 3)-sidechains have also been found. Acidic AXs are present in the outer tissues of cereal grains. They carry α(1 → 2)-linked glucopyranosyluronic acid or 4-*O*-methyl-glucopyranosyluronic acid substituents. Feruloyl residues linked to Ara*f* residues are also found. The number of substituents is known to vary in different cereals, tissues, and even in tissue layers (Saulnier et al., 2007). Since structural features are related to physicochemical properties, such as water solubility, viscosity, and gelation (Saulnier, Sado, Branlard, Charmet, & Guillon, 2007), identification of the structure of AX is important if it is added to baking products or exploited in other industrial applications.

The structural analysis of large polysaccharide molecules is challenging; therefore, AXs are commonly hydrolyzed into (A)XOS prior to analysis. Nuclear magnetic resonance (NMR) spectroscopy (Duus, Gotfredsen, & Bock, 2000), high-performance anion-exchange chromatography with pulsed amperometric detection (HPAEC-PAD) (Pastell, Tuomainen, Virkki, & Tenkanen, 2008, Pastell, Virkki, Harju, Tuomainen, & Tenkanen, 2009), and gas chromatography-mass spectrometry (GC–MS) analysis of methylated (A)XOS (Ciucanu, 2006) have been popular techniques for the structural characterization of (A)XOS. The last two decades have seen an increased interest in using mass spectrometry (MS) and tandem mass spectrometry (MS/MS) for the structural analyses of carbohydrates (Mischnick, 2011). One specific benefit of MS and MS/MS analyses is that they require only small amounts of a sample to achieve a very sensitive analysis. Matrix-

* Corresponding author.
E-mail address: minna.juvonen@helsinki.fi (M. Juvonen).

https://doi.org/10.1016/j.foodchem.2018.09.074
Received 20 April 2018; Received in revised form 7 September 2018; Accepted 11 September 2018
Available online 12 September 2018

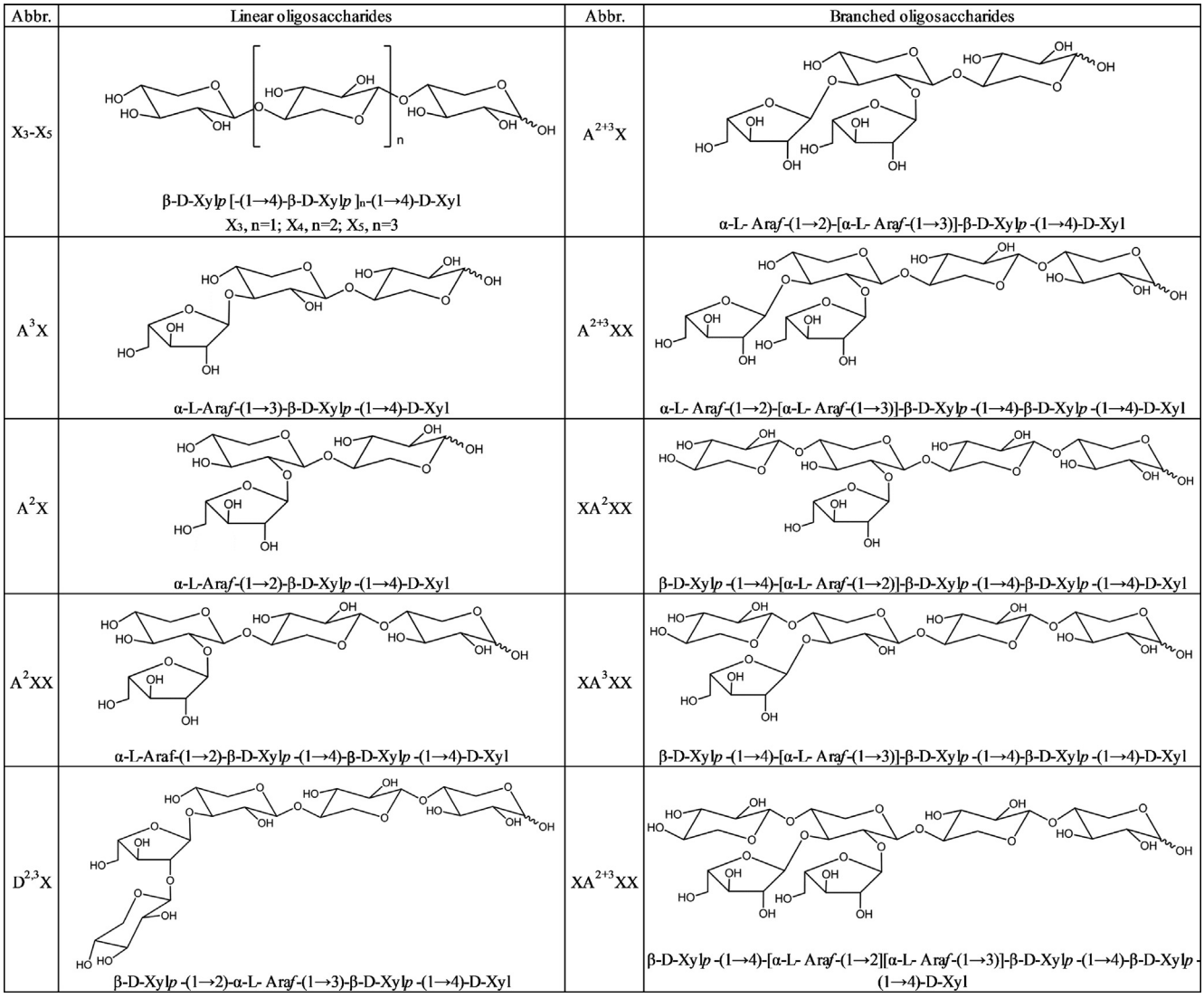

Fig. 1. The structural models and abbreviations of xylooligosaccharide and arabinoxylooligosaccharide samples (XOS and AXOS). Abbreviations of AXOS by Fauré et al. (2009).

assisted laser desorption ionization mass spectrometry (MALDI-MS) has been shown to be an efficient tool for determining the molecular weight distribution of (A)XOS. Reverse-phase high-performance liquid chromatography (RP-HPLC) combined with MS/MS has been used for the structural characterization of derivatized (A)XOS (Bowman, Dien, Vermillion, & Mertens, 2014). Recent and novel stationary phases, such as porous graphitized carbon (PGC) and hydrophilic interaction liquid chromatography (HILIC) phases, have enabled the HPLC-MS or HPLC-MS/MS analysis of oligosaccharides without derivatization (Everest-Dass, Kolarich, Campbell, & Packer, 2013, Everest-Dass et al., 2013, Hernandez-Hernandez, Calvillo, Lebron-Aguilar, Moreno, & Sanz, 2012, Leijdekkers, Sanders, Schols, & Gruppen, 2011, Leijdekkers et al., 2011, Liu, Kisonen, Willför, Xu, & Vilaplana, 2016, Liu et al., 2016, Pu, Zhao, Xiao, & Zhao, 2017).

Positive ion MS/MS can determine linkage positions and sequences of different oligosaccharides (Asam & Glish, 1997, Hofmeister, Zhou, & Leary, 1991, Mischnick, 2011). However, in MS/MS, positively charged oligosaccharide ions fragment from both ends, and, if the oligosaccharides consist of the same mass monomers, such as (A)XOS, identification of isobaric fragment ions is difficult and sometimes even impossible. Therefore, derivatization techniques, such as derivatization by per-*O*-methylation (Ciucanu, 2006, Matamoros Fernández, Obel, Scheller, & Roepstorff, 2003) and labeling the reducing end, for example, with ^{18}O isotope (Hofmeister et al., 1991) or reagents (Suzuki, 2013), have commonly been used to differentiate the reducing end and non-reducing end fragment ions.

However, some studies have indicated that derivatization may not be needed if negative ionization is used. Negatively charged oligosaccharides have been reported to fragment mainly from the reducing end towards the non-reducing end and produce non-reducing end consisting ions (A-, B-, and C-ions) (Carroll, Willard, & Lebrilla, 1995, Chai, Piskarev, & Lawson, 2001, Harvey, 2005, Maina et al., 2013, Pfenninger, Karas, Finke, & Stahl, 2002a). Fragmentation in one direction can facilitate the analysis of cross-ring fragments from middle residues (Maina et al., 2013). By analyzing the cross-ring fragments, the linkages have been determined from negatively charged deprotonated (Harvey, 2005, Pfenninger et al., 2002a) or anion adduct (Guan & Cole, 2008, Zhu & Cole, 2001) disaccharides and oligosaccharides.

Although negative ionization MS/MS methods have been widely developed for the structural analysis of oligosaccharides, to our knowledge, only two MS/MS studies of AXOS using negative ionization have been published. Quemener, Ordaz-Ortiz, and Saulnier (2006) characterized the structure of neutral deprotonated AXOS by electrospray ionization quadrupole time-of-flight mass spectrometry (ESI-Q-TOFMS) and electrospray ionization ion trap mass spectrometry (ESI-ITMS). They showed that mono- or di-substituted AXOS (*O*-3-

substituted *vs*. *O*-3- and *O*-2-substituted) can be differentiated by the negative ion MS/MS method. Wang et al. (2009) developed the negative ion HPLC-MS^n method for structure elucidation of feruloylated AXOS. In both studies, the AX was hydrolyzed by glycoside hydrolase family 11 (GH11) endoxylanase. GH11 endoxylanases cleave the xylan backbone but not near the branching residues. Therefore the AXOS have unsubstituted +1 Xyl*p* residues and +2 branched residues (Pollet, Delcour, & Courtin, 2010). Other common endoxylanase enzymes, which are also present endogenously in plants, hydrolyzing AX, are GH10 family enzymes. GH10 endoxylanases cleave the AX backbone near the branching residue (+1 being branched residue), and they form AXOS without the *O*-4 linked backbone Xyl*p* residue at the non-reducing end. We think that the development of an MS/MS method for structural analysis for the GH10 hydrolyzed AXOS is clearly needed. As AXOS are usually hydrolysate mixtures of AX, combining the negative MS/MS method with HILIC would enable high-throughput analysis of AXOS mixtures without sample derivatization.

In this study, we present a novel negative ionization HILIC-MS/MS method for the analysis of the linkage positions and branching points of AXOS. The present work achieves the following: 1) to elucidate the fragmentation behavior of chlorinated AXOS in negative electrospray ionization multiple-stage mass spectrometry (ESI-MS^n), 2) to determine how linkage positions influence the fragmentation of linear and branched AXOS, and 3) to ascertain the identification of linear and branched AXOS by negative ion HILIC-MS/MS. Since our samples included AXOS from both GH10 and GH11 family hydrolysates, they comprise all possible linkage positions and branches that AXOS can form, including also the rare β-D-Xyl*p*-(1 → 2)-α-L-Ara*f*-(1 → 3)-β-D-Xyl*p*-(1 → 4)-Xyl*p* and α-L-Ara*f*-(1 → 2)-mono-substituted samples.

2. Materials and methods

2.1. Samples and chemicals

Five linear XOS (X_1, X_2, X_3, X_4, and X_5,) and three branched AXOS samples (XA^3XX, XA^2XX + XA^3XX, and $XA^{2+3}XX$, named GH11 AXOS) were purchased from Megazyme International (Bray, Ireland). Six AXOS samples (A^2X, A^3X, $A^{2+3}X$, $A^{2+3}XX$, A^2XX, and $D^{2,3}X$, named GH10 AXOS) were prepared earlier by our group, as published elsewhere (Pastell et al., 2008, Pastell et al., 2009, Rantanen et al., 2007). The structures of the AXOS and XOS samples are shown in Fig. 1. Abbreviations are by Fauré et al. (2009). The A^3X, $A^{2+3}X$, $A^{2+3}XX$, A^2X, and A^2XX were prepared from wheat arabinoxylan (Megazyme International, Bray, Ireland) and the $D^{2,3}X$ from oat spelt arabinoxylan (Sigma Aldrich Chemie, Steinheim, Germany) by using different hydrolyzing enzyme treatments. In short, the treatments included enzymatic hydrolysis by GH family 10 endo-1,4-*β*-D-xylanase (Shearzyme; Novozymes, Bagsvaerd, Denmark), GH family 51 *α*-L-arabinofuranosidase (Megazyme International, Bray, Ireland), and GH family 43 *α*-L-arabinofuranosidase (Megazyme International, Bray, Ireland). Hydrolysates were fractionated by gel permeation chromatography (GPC) and identified by HPAEC-PAD and NMR spectroscopy. All chemicals were of analytical grade unless otherwise stated.

2.2. Direct infusion ESI-MS^n

The positive and negative ion MS^n spectra of AXOS samples were produced by the Agilent XCT Plus model ion trap mass spectrometer (Agilent Technologies, Waldbronn, Germany) equipped with an electrospray ionization (ESI) source. The parameters were as reported previously (Maina et al., 2013), except the electrospray capillary voltage was set to (±) 3200 V. The samples were diluted in methanol/water/formic acid (50/49/1, *v/v/v*) to a final concentration of 8–12 μg/mL. The samples were directly infused into the ion source at a flow rate of 5 μL/min. Ammonium chloride (NH_4Cl, 40 μg/ml) was added in negative ionization mode for $[M + Cl]^-$ adduct ion formation.

2.3. HILIC-MS/MS method development

2.3.1. Optimization of ion trap parameters

XOS standards (X_1–X_5) were analyzed using a Bruker Esquire quadrupole ion trap (Bruker, Bremen, Germany) equipped with an ESI source and using direct infusion (5 μL/min) and negative ionization. Samples of 10 μg/mL were prepared in 80% acetonitrile (ACN) with 0.1% NH_4OH. NH_4Cl (50 μg/mL) was added for chloride adduct formation. Ion trap parameters with the highest intensity level were optimized for each standard. The optimized fragmentation amplitudes were 0.65 V for X_2, 0.60 V for X_3, 0.70 V for X_4 and 0.55 V for X_5. For $XA^{2+3}XX$ the 0.5 V fragmentation amplitude was used.

2.3.2. HPLC setup

Optimized ion trap parameters were tested by HILIC-MS with a mixture of four XOS (X_2-X_5) and six AXOS samples. The chromatographic separation was performed with HPLC (Agilent 1100 Series HPLC, Agilent Technologies, Santa Clara, CA) on a 3.5 μm, 2.1 × 150 mm Xbridge BEH amide column (Waters, Milford, MA). The mobile phases were A) 80% ACN with 0.1% ammonium hydroxide (NH_4OH) and B) 20% ACN with 0.1% NH_4OH. The mobile phase elution profile was as follows: 80% ACN to 50% ACN in 31 min, isocratic (50% ACN) for 5 min, back to initial conditions in 1 min, and 15 min washing in initial conditions (based on Brokl, Hernández-Hernández, Soria and Sanz (2011)). Flow rate was 200 μL/min and oven temperature was set to 35 °C. Injection volume was 10 μL. The segment program was created for HILIC-MS. The segments were the following: 0–7 min with X_2 parameters, 7–12 min with X_3 parameters, 12–17 min with X_4 parameters, 17–23 min with X_5 parameters, and 23–31 min with X_5 parameters.

2.3.3. Optimization of post-column NH_4Cl addition parameters

The chloride adduct ions were formed by adding NH_4Cl (in 80% ACN with 0.1% NH_4OH) post-column to the mobile phase flow via a mixing tee with an HPLC pump (Waters 501 HPLC system; Millipore, Milford, MA). Post-column addition of NH_4Cl was tested with flow rates of 100 μL/min and 200 μL/min and NH_4Cl concentrations of 1 μg/mL, 2.5 μg/mL, 5 μg/mL, 7.5 μg/mL, and 10 μg/mL. Testing was performed with 5 μg/mL and 10 μg/mL XOS mixture (X_2–X_5) solutions. The aim was to determine the lowest concentration of NH_4Cl that produces the maximal $[M + Cl]^-$ adduct ion signal.

2.3.4. HILIC-MS/MS of AXOS samples

The HILIC-MS/MS methods were set up for tri-, tetra-, penta- and hexasaccharides by optimized ion trap parameters and fragmentation amplitudes. The chloride adduct ions were formed by adding NH_4Cl post-column in an optimized concentration and flow rate (10 μg/mL in 80% ACN with 0.1% NH_4OH, 200 μL/min). The MS and MS^2 spectra were produced from all samples.

3. Results and discussion

3.1. Linkage determination of linear XOS and AXOS by direct infusion ESI-MS^n

The first part of the study was to find out how the XOS and AXOS linkage positions reflect on the product ion spectra. The negative ion MS^2 and MS^3 spectra of the linear XOS and AXOS are shown in Fig. 2. Product ions are named according to Domon and Costello (1988).

3.1.1. Determining the (1 → 4)-linkage

All the commercial XOS samples consisted of β(1 → 4)-linked Xyl*p* residues. The MS^2 spectrum of X_4 shows that the reducing end Xyl*p* residue formed $^{0,2}A$ and $^{0,2}A$-H_2O cross-ring fragment ions at *m/z* 485 and *m/z* 467 (Fig. 2a). The (1 → 4)-linked middle residues fragmented to $^{0,2}A_3$-ions (*m/z* 353) and $^{0,2}A_3$-H_2O-ions (*m/z* 335) as well. All the

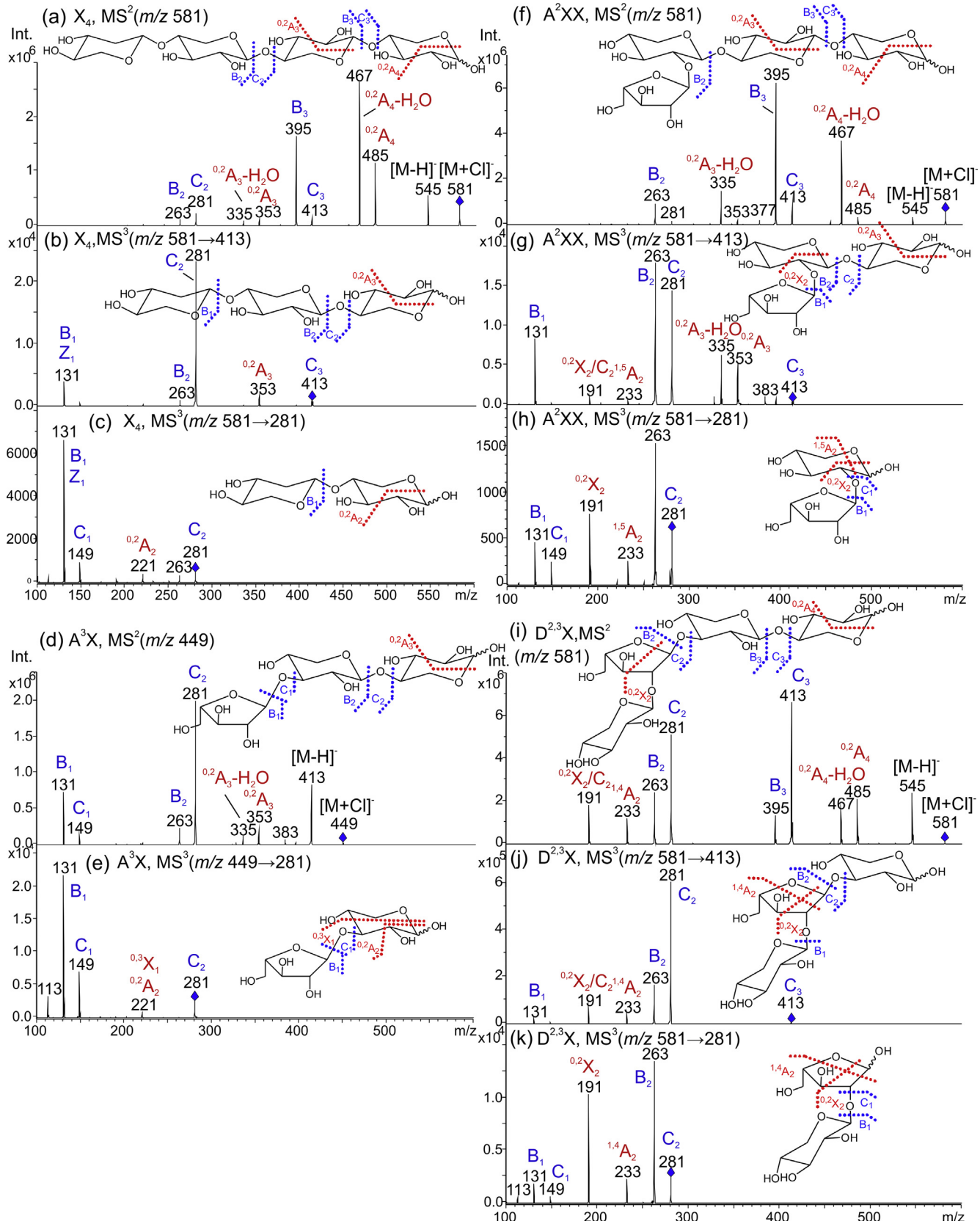

Fig. 2. Negative ion MS^n spectra of linear (A)XOS samples and characterization of fragmentation. Precursor ions are $[M + Cl]^-$ and product ions are deprotonated. / = double cleavage. (a) X_4, MS^2 *m/z* 581, (b) X_4, MS^3 *m/z* 581 → 413, (c) X_4, MS^3 *m/z* 449 → 281, (d) A^3X, MS^2 *m/z* 449, (e) A^3X, MS^3 *m/z* 449 → 281, (f) A^2XX, MS^2 *m/z* 581, (g) A^2XX, MS^3 *m/z* 581 → 413, (h) A^2XX, MS^3 *m/z* 581 → 281, (i) $D^{2,3}X$, MS^2 *m/z* 581, (j) $D^{2,3}X$, MS^3 *m/z* 581 → 413, and (k) $D^{2,3}X$, MS^3 *m/z* 581 → 281. Product ions named according to Domon and Costello (1988).

linear GH10 AXOS samples were also found to produce ^{0,2}A and ^{0,2}A-H_2O cross-ring fragment ions from their (1 → 4)-linked reducing ends in MS^2 (A^2XX: *m/z* 485 and *m/z* 467 in Fig. 2f; A^3X: *m/z* 353 and *m/z* 335 in Fig. 2d, and $D^{2,3}X$: *m/z* 485 and *m/z* 467 in Fig. 2i). This was an expected result, since many studies of negatively charged oligosaccharides have reported the (1 → 4)-linked oligosaccharides fragmenting by ^{0,2}A and ^{0,2}A-H_2O cross-ring cleavages (Pfenninger, Karas, Finke, & Stahl, 2002b, Zhu & Cole, 2001), and this has also been observed in deprotonated (A)XOS (Quemener et al., 2006, Wang et al., 2009). The C_2-ions and C_3-ions were isolated and further fragmented in MS^3. The C_3-ions and C_2-ions of commercial X_4, which contained (1 → 4)-linkage at the reducing end, were again found to produce ^{0,2}A-ions (*m/z* 353 in Fig. 2b and *m/z* 221 in Fig. 2c), but the ^{0,2}A-H_2O cross-ring ions were not formed. The (1 → 4)-linked C_3-ions of A^2XX fragmented to both ^{0,2}A- and ^{0,2}A-H_2O-ions in MS^3 (*m/z* 335 and *m/z* 353 in Fig. 2g).

3.1.2. Determining the (1 → 2)-linkage

The C_3-ions and C_2-ions of A^2XX produced cross-ring fragment ions with *m/z* 191 (C_2-90 Da) and *m/z* 233 (C_2-48 Da) in MS^3 (Fig. 2g-h). We suggest that the *m/z* 191 is a $^{0,2}X_2$-ion, since the (1 → 2)-linked hexose oligosaccharides have been found to fragment by ^{0,2}X-type ions due to the loss of 120 Da neutrals (Maina et al., 2013). The *m/z* 233 could be a $^{1,5}A_2$-ion, formed by the loss of the reducing end of the C_2-ion. As expected, the same cross-ring ion peaks were seen in the spectra of $D^{2,3}X$, which also contained (1 → 2)-linked middle residue (*m/z* 191: ^{0,2}X and *m/z* 233: ^{1,4}A in Fig. 2j-k). It was also noted that the MS^3 spectrum of the C_2-ion of $D^{2,3}X$ (Fig. 2k) was nearly identical to the MS^3 spectrum of the C_2-ion of A^2XX (Fig. 2h). Therefore, we suggest that the M-90 Da (^{0,2}X) and M-48 Da (^{1,4}A if Ara*f* and ^{1,5}A if Xyl*p*) cross-ring cleavages are diagnostic for (1 → 2)-linkages in pentoses. Unfortunately, the method is not capable of differentiating β-D-Xyl*p*-(1 → 2)-α-L-Ara*f* from α-L-Ara*f*-(1 → 2)-β-D-Xyl*p*.

3.1.3. Determining the (1 → 3)-linkage

The A^3X (Fig. 2d) and $D^{2,3}X$ (Fig. 2i), which had (1 → 3)-linkages between their middle residues, did not form ^{0,2}A, or any other kind of cross-ring fragments from *O*-3-position linked residues. The finding that (1 → 3)-linked oligosaccharides do not fragment via cross-ring cleavages in negative mode is consistent with the results of deprotonated AXOS (Quemener et al., 2006). In MS^3, the C_3-ion of $D^{2,3}X$, which had a (1 → 3)-linked reducing end residue, did not produce cross-ring fragments from the reducing end residue (Fig. 2j). However, in the C_2-ion spectrum of (1 → 3)-linked A^3X, a small number of the cross-ring ions were observed with *m/z* 221 (Fig. 2e). The spectrum was very similar to the C_2-ion spectrum of the (1 → 4)-linked X_4 (Fig. 2c), but did not have a loss of water peak (*m/z* 263). These cross-ring ions are most likely $^{0,3}X_1$-ions, since we have experienced that deprotonated (1 → 3)-linked hexose disaccharides form $^{0,3}X_1$-ions by the loss of 90 Da units (Juvonen, 2011). On the other hand, the chlorinated (1 → 3)-linked hexose disaccharides were observed to lack the cross-ring fragmentation (Maina et al., 2013). These differences in fragmentation of (1 → 3)-linked deprotonated and chlorinated ions should be kept in mind if interpreting spectra of unknown oligosaccharides.

3.2. Structural analysis of branched AXOS by direct infusion ESI-MS^n

The analysis continued by examining how branching points of AXOS influence on fragmentation. The negative ion MS^2 spectra of branched AXOS are shown in Fig. 3. As XA^2XX was available only as part of the mixture, the MS^2 spectrum of XA^2XX is from HILIC-MS/MS.

3.2.1. Determining the (1 → 4)-linkages from linear parts of branched AXOS

In MS^2, as observed previously with linear (A)XOS, the branched GH11 AXOS samples also formed ^{0,2}A and ^{0,2}A-H_2O type cross-ring fragment ions from their (1 → 4)-linked linear reducing end residue (*m/z* 749 and *m/z* 731 in Fig. 3a; *m/z* 617 and *m/z* 599 in Fig. 3b-c). Furthermore, ^{0,2}A and ^{0,2}A-H_2O cross-ring fragment ions were formed from (1 → 4)-linked middle residues (*m/z* 617 and *m/z* 599 in Fig. 3a; *m/z* 485 and *m/z* 467 in Fig. 3b-c). Also, as expected, the branched GH10 AXOS, $A^{2+3}XX$, and $A^{2+3}X$ fragmented from their (1 → 4)-linked xylan backbone by ^{0,2}A and ^{0,2}A-H_2O type cross-ring cleavages (*m/z* 617, *m/z* 599, *m/z* 485, and *m/z* 467 in Fig. 3d-e).

3.2.2. Branching point determination of AXOS by MS^2

The hypothesis was that, if the branched AXOS followed the same fragmentation behavior as linear AXOS and started fragmenting from the reducing end, the branching points could be determined by a lack of cross-ring ions in the spectrum. However, it was found that the lack of ions was observed only in the spectra of the Ara*f* mono-substituted GH11 AXOS samples (XA^2XX in Fig. 3b; XA^3XX in Fig. 3c) between *m/z* 281 and *m/z* 395. The di-substituted $XA^{2+3}XX$ showed a peak at *m/z* 467 (Fig. 3a), even though the spectrum should have been lacking ions between *m/z* 395 and *m/z* 527, if it has been fragmented only from the reducing end. The ions at *m/z* 467 were characterized as $^{0,2}A_4/Y_{3x}$-ions formed by co-fragmentation of the reducing and the non-reducing ends. Interestingly, the branched GH10 AXOS, $A^{2+3}XX$, and $A^{2+3}X$ were also found to co-fragment from both ends, similarly to the Ara*f* di-substituted $XA^{2+3}XX$; therefore, no lack of ions indicating branching residue were shown in their spectra either (*m/z* 323 and *m/z* 335 in Fig. 3d-e). The peak was characterized at *m/z* 323 as a $^{2,4}A_3/Y_{3x}$-ion and at *m/z* 335 as a ^{0,2}A-H_2O/Y_{3x}-ion. Di-substituted samples fragmenting from both ends implies that di-substitution enhances the Y-type fragmentation of Ara*f* substituents.

3.2.3. Characterization of branched AXOS by MS^2

The Ara*f* mono-substituted pentasaccharides XA^3XX and XA^2XX were easily differentiated from each other by the peak at *m/z* 299 in the spectrum of XA^3XX (Fig. 3c). It was reported earlier that *O*-3-branched AXOS produce these unique types of ions by double C- and Y-type cleavages combined with a water molecule addition in the negative mode (Quemener et al., 2006). Therefore, the *m/z* 299 was characterized as C_2/Y_{3x} + H_2O-ions. Since these fragment ions were absent also in the MS^2 spectrum of pentasaccharide $A^{2+3}XX$ (Fig. 3d), the peak at *m/z* 299 is an excellent indicator of XA^3XX.

The Ara*f* di-substituted sample $XA^{2+3}XX$ (Fig. 3a) was found to produce more abundant *m/z* 587 (C-90 Da) compared to the mono-substituted samples XA^2XX and XA^3XX (Fig. 3b-c). Since the cross-ring fragmentation most likely happens from the reducing end toward the non-reducing end by retro-aldol reaction, it is likely ^{2,4}A-ion. The same ^{2,4}A-type ions were found from spectra of branched GH10 AXOS samples: *m/z* 587 and *m/z* 455 in $A^{2+3}XX$ (Fig. 3d) and *m/z* 455 and *m/z* 323 in $A^{2+3}X$ (Fig. 3e). It should be noted that the linear samples Xyl*p* backbone did not fragment by these cross-ring cleavages.

The branched, Ara*f* di-substituted $A^{2+3}XX$ (Fig. 3d) and $A^{2+3}X$ (Fig. 3e) both produced peaks at *m/z* 263 in MS^2. Since the *m/z* 263 was not found in the MS^2 spectra of the branched Ara*f* mono-substituted pentasaccharides XA^2XX or XA^3XX, the $A^{2+3}XX$ can be distinguished by it. The peak is probably formed by D-type glycosidic bond fragment ions (C_2/Z_{3x}-ions). The D-ions have been reported to fragment from some *O*-3-branched oligosaccharides next to the *O*-3-branching unit by double C- and Z-cleavages in negative mode (Chai et al., 2001, Chai, Lawson, & Piskarev, 2002, Everest-Dass et al., 2013, Harvey, 2005). The assumed D-ions were also found in the MS^2 spectra of di-substituted $XA^{2+3}XX$ (*m/z* 395, Fig. 3a). Since the D-ions are also isobaric to B-ions formed from linear AXOS, they cannot, however, act as an indicator of di-substituted or branched structures.

3.2.4. Characterization of branched AXOS by MS^3

The C_2- and C_3-ions of branched samples were isolated and fragmented in MS^3. The precursor ions might have consisted of some minor

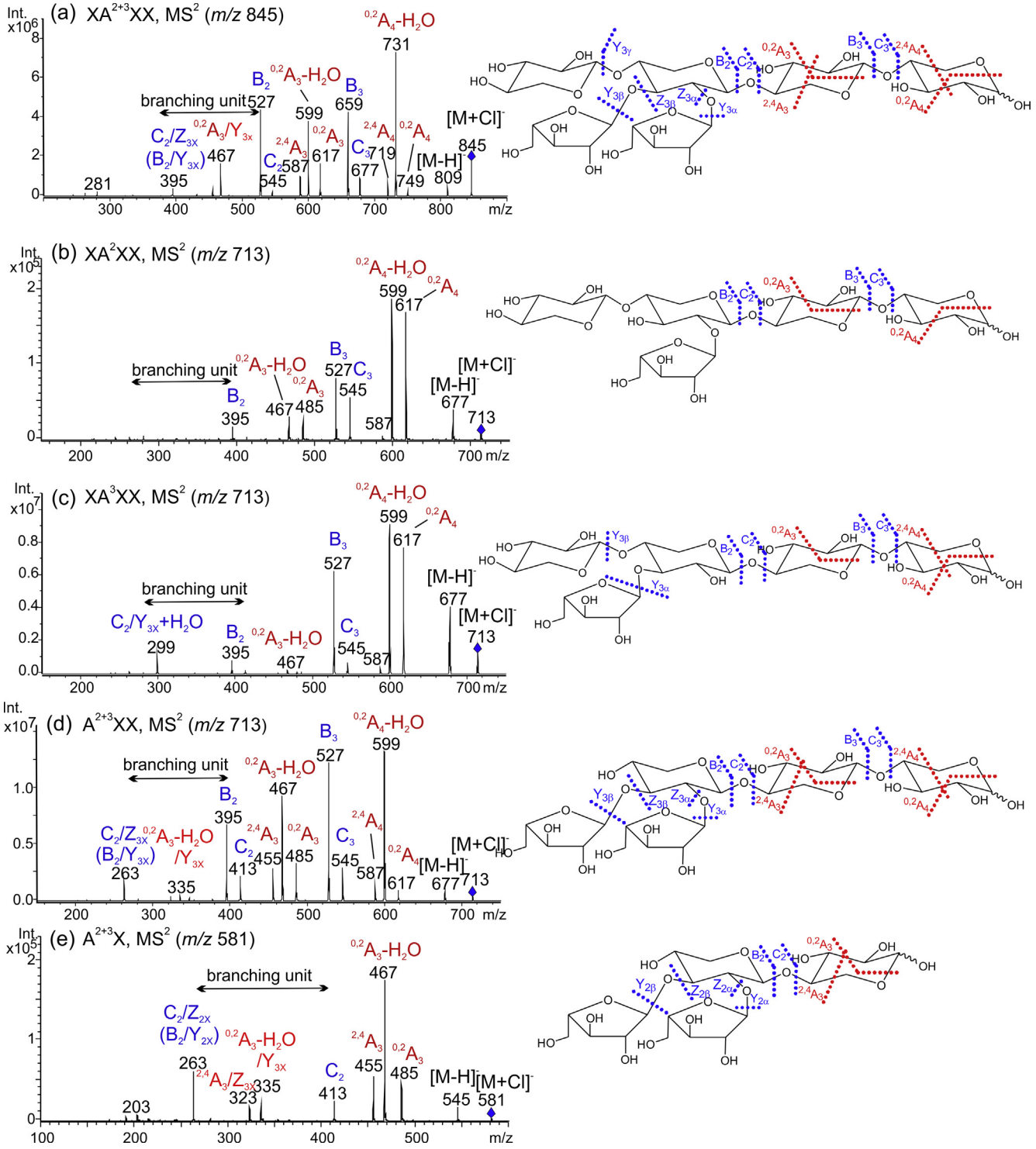

Fig. 3. Negative ion MS^2 spectra of the branched AXOS and characterization of fragmentation. Precursors are $[M + Cl]^-$ adduct ions. Product ions are deprotonated. / = double cleavage, x = α, β, or γ; branching unit = the *m/z* area of branching unit if fragmentation from reducing end. (a) $XA^{2+3}XX$, *m/z* 845, (b) XA^2XX (HILIC-MS^2), *m/z* 713, (c) XA^3XX, *m/z* 713, (d) $A^{2+3}XX$, *m/z* 713, and (e) $A^{2+3}X$, *m/z* 581. Product ions named according to Domon and Costello (1988).

proportion of Y-ions, since non-reducing end fragmentations were detected in MS^2. Each MS^3 spectrum of branched AXOS was observed to be different from the others (Fig. 4). This means that all these branched tri- or tetrasaccharide ions could be identified by the MS^3 spectrum. For example, the C_2-ion of $XA^{2+3}XX$ (Fig. 4b) showed peaks at *m/z* 431 and *m/z* 395. The spectra of the C_2- and C_3-ions of XA^3XX had abundant peaks at *m/z* 299 (Fig. 4d-e) which were absent in other spectra. The C_3-ion spectrum of $A^{2+3}XX$ showed ^{2,4}A-ions at *m/z* 455 but was lacking the B_2-ions at *m/z* 395. The C_2-ion spectrum had a strong peak at *m/z* 263, but showed no peak at *m/z* 299. The C_3-ion spectrum of XA^2XX (Fig. 4c) was lacking both the *m/z* 299 and *m/z* 431, but had an abundant B_2-ion peak at *m/z* 395.

The ions with *m/z* 299, which were earlier identified as $C_2/Y_{3x} + H_2O$ in the MS^2 of XA^3XX, were found also in the MS^3 spectra of XA^3XX (Fig. 4d-e). A surprising finding was the peak at *m/z* 431, which was found in the C_2-ion spectrum of $XA^{2+3}XX$ (Fig. 4b) and in the C_3-

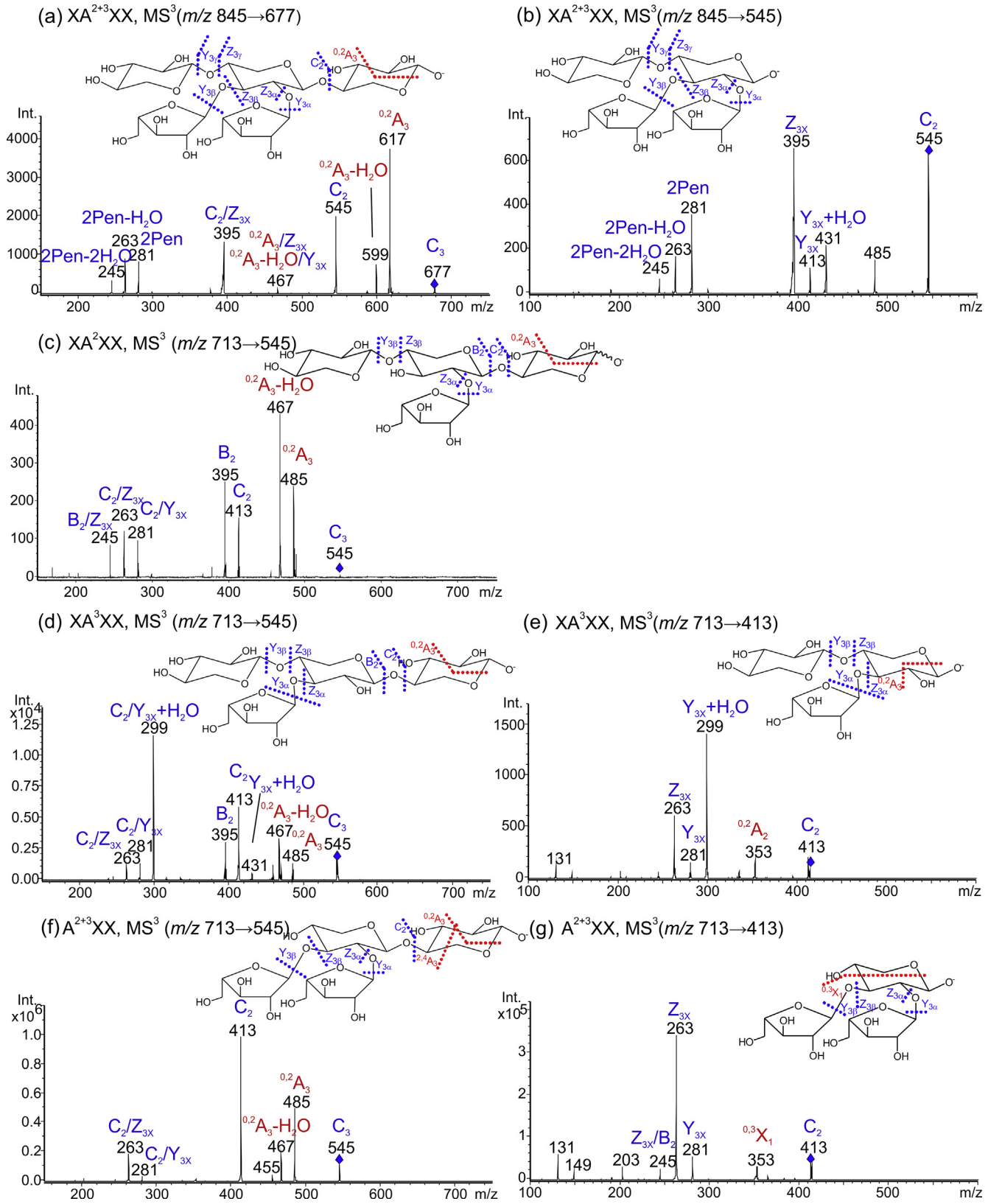

Fig. 4. Negative ion MS^3 spectra of the branched AXOS' C_3- and C_2-ions and characterization of fragmentation. Precursors are $[M + Cl]^-$ adduct ions, and product ions are deprotonated. (a) $XA^{2+3}XX$, *m/z* 845 → 677, (b) $XA^{2+3}XX$, *m/z* 845 → 545, (c) XA^2XX, *m/z* 713 → 545, (d) XA^3XX, *m/z* 713 → 545, (e) XA^3XX, *m/z* 713 → 413, (f) $A^{2+3}XX$, *m/z* 713 → 545, and (g) $A^{2+3}XX$, *m/z* 713 → 413. Product ions named according to Domon and Costello (1988).

ion spectrum of XA^3XX (Fig. 4d). These fragment ions are one pentose unit larger than the ions at *m/z* 299, and, therefore, they are also assumed to be $C/Y_{3x} + H_2O$ ions. Both of these ions (*m/z* 299 and *m/z* 431) were only found in the spectra of *O*-4- and *O*-3-branched samples. We suggest that a water molecule has been added to the C-ion after the Y-type cleavage of (1 → 3)-linked Ara*f* or (1 → 4)-linked Xyl*p* residues from the non-reducing end, as then the ring has the potential to open with the formation of an aldehyde, which is known to react with water to form a hydrate.

The fragment ions, which we earlier suggested to be D-ions (C_2/Z_{3x}-ions), were observed in all MS^3 spectra of the *O*-3-branched samples. We assume them to be D-ions, not Z-ions, because Quemener et al. (2006) reported the same *m/z* at the spectrum of deprotonated XA^3X, when the reducing end was differentiated from the non-reducing end by ^{18}O-labelling. The D-ions were found in the MS^3 of $XA^{2+3}XX$ (Fig. 4a-b, *m/z* 395), XA^3XX (Fig. 4d-e, *m/z* 263), and $A^{2+3}XX$ (Fig. 4f-g, *m/z* 263). Unfortunately, the *m/z* 263 was also found from the spectrum of *O*-2-branched XA^2XX (Fig. 4c), and, therefore, it cannot be a diagnostic peak of the *O*-3-linked branch. As previously commented, the D-ions are also isobaric to B-ions formed from linear AXOS; thus, they cannot act as an indicator of the branched structure either.

Interestingly, the MS^3 spectra were observed to also contain other kinds of double cleavage fragment ions. These ions were found as minor peaks at *m/z* 245 and were formed only from *O*-2-branched samples ($XA^{2+3}XX$ in Fig. 4a-b, XA^2XX in Fig. 4c, and $A2^{+3}XX$ in Fig. 4g). These could be E- or F-type elimination ions as previously reported (Maslen, Goubet, Adam, Dupree, & Stephens, 2007, Spina et al., 2004) and formed by double B- and Z-cleavages (E-type) or two Z-cleavages (F-type). Since linear AXOS did not form these ions in MS^3, the ions at *m/z* 245 are the potential diagnostic peaks of the branched structure. However, more research is needed to determine if the more complicated branched samples also fragment similarly.

3.3. Analysis of (A)XOS by positive ESI-MS^n

To show the difference between positive and negative ionization, the positive MS^2 and MS^3 spectra of three lithium cationized tetrasaccharides (X_4, $D^{2,3}X$, and $A^{2,3}X$) are presented in Online Resource 1 (OR. 1). The branched $A^{2,3}X$ was observed to produce primarily the same peaks in MS^2 as the linear equivalents X_4 and $D^{2,3}X$. The only exception was a peak at *m/z* 253 in the $A^{2,3}X$ spectrum (OR. 1e). Otherwise, only differences in the ion intensity occurred. All three samples were found to produce $^{0,2}A$ cross-ring fragments (*m/z* 493, neutral loss of 60 Da) from their (1 → 4)-linked reducing end residues. A small peak of the $^{2,4}A$-ion (*m/z* 463, neutral loss of 90 Da) was also observed. The same $^{0,2}A$- and $^{2,4}A$-type of cross-ring fragment ions were formed in MS^3 (*m/z* 361, *m/z* 331, and *m/z* 229) from the Y- and C-ions (OR. 1b, 1d, and 1f). Since the three MS^3 spectra were very similar, the isolated ions for MS^3 had to be mainly Y-ions formed by losing a non-reducing end. It was clear that the positive ion ESI-MS^n was not as effective as the negative ion ESI-MS^n to characterize the structural differences of (A)XOS samples which were located near the non-reducing end.

3.4. HILIC-MS/MS

3.4.1. Setting up HILIC-MS in negative mode

Based on the promising results in negative ionization, implementation of the chromatographic method with an HILIC column was initiated by using negative ionization. In the first phase, the ion trap parameters were optimized for every XOS standard (X_1-X_5) by using direct infusion. Then, the optimized parameters were tested by HILIC-MS with XOS and AXOS samples. The chromatograms of the XOS mixture (X_2-X_5) analyzed with different parameters can be found in OR. 2. It was observed that larger oligosaccharides formed smaller peaks when optimized parameters for X_2 and X_3 were used, and smaller oligosaccharides formed smaller peaks on X_3-X_5 optimized parameters. As a result, the segment program was applied for MS. The segment program changes the ion trap parameters during the run, to obtain the highest intensity levels (Fig. 5a).

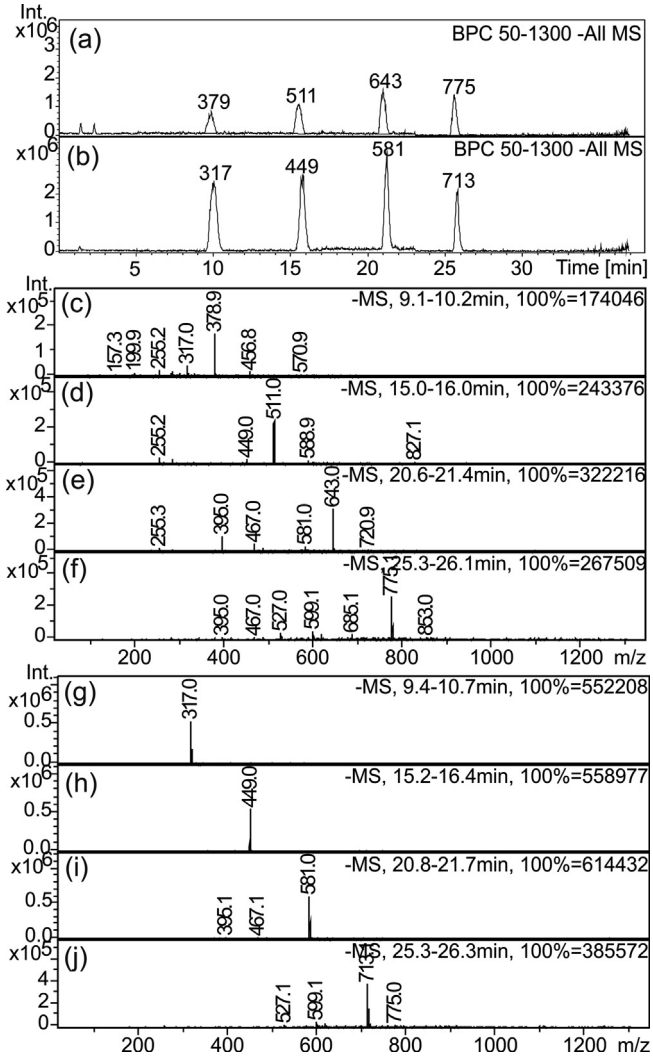

Fig. 5. Optimization of post-column addition of NH_4Cl to HILIC-MS with X_2-X_5 samples. Segment program: (a) Base peak chromatogram of X_2-X_5 mixture, without NH_4Cl addition, (b) Base peak chromatogram of X_2-X_5 mixture, 10 μg/l NH_4Cl added with flow rate 200 μL/min, (c-f) HILIC-MS spectrum of X_2, X_3, X_4 and X_5, respectively, without NH_4Cl addition, (g-j) HILIC-MS mass spectrum of X_2, X_3, X_4, and X_5, respectively, 10 μg/L NH_4Cl added with flow rate of 200 μL/min.

The MS spectra of samples showed that various adduct ions were formed in the negative ionization mode (Fig. 5c-f). The intensity levels of base peaks were approximately 2×10^5–3×10^5. NH_4Cl was added to form exclusively chloride adducts and to enhance the intensity level. The post-column addition of NH_4Cl was chosen to enable the use of the same mobile phase in the positive mode. Post-column addition was tested with two flow rates and five concentrations of NH_4Cl. The smallest concentration to form acceptable peaks was found to be 10 μg/mL with a flow rate of 200 μL/min (Fig. 5b). The $[M + Cl]^-$ adduct ions were observed to be the dominant peaks in the MS spectra of XOS (*m/z* 317, *m/z* 449, *m/z* 581, and *m/z* 713 in Fig. 5g-j). Furthermore, the addition of NH_4Cl increased the intensity level of base peaks to 4×10^5–6×10^6.

3.4.2. HILIC-MS/MS of (A)XOS

In the last stage of the study, the (A)XOS samples were analyzed by

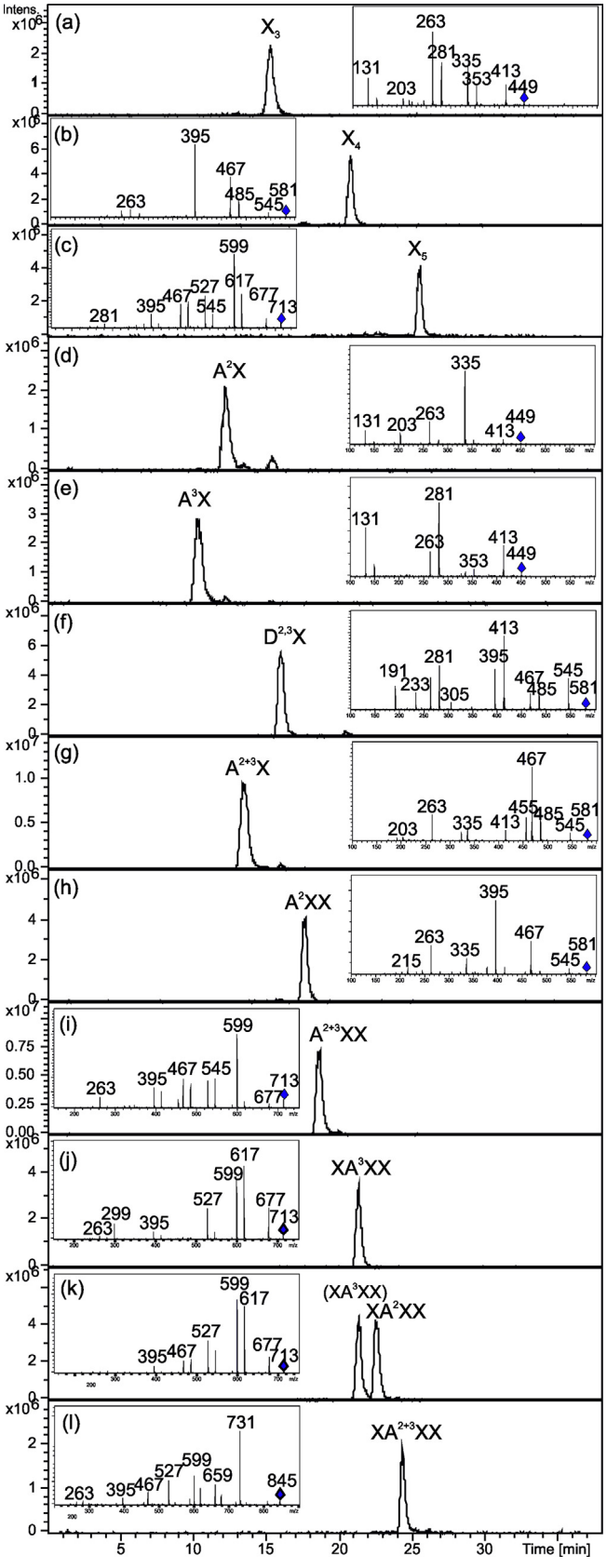

Fig. 6. Extracted ion chromatograms of (A)XOS analyzed by negative ion HILIC-MS and MS^2 spectra of HILIC-MS/MS. Precursors are [M + Cl] – adduct ions and product ions are deprotonated. (a) X_3, MS^2 *m/z* 449, (b) X_4, MS^2 *m/z* 581, (c) X_5, MS^2 *m/z* 713, (d) A^2X, MS^2 *m/z* 449, (e) A^3X, MS^2 *m/z* 449, (f) $D^{2+3}X$, MS^2 *m/z* 581, (g) $A^{2+3}X$, MS^2 *m/z* 581, (h) A^2XX, MS^2 *m/z* 581, (i) $A^{2+3}XX$, MS^2 *m/z* 713, (j) XA^3XX, MS^2 *m/z* 713, (k) XA^2XX, MS^2 *m/z* 713, and (l) $XA^{2+3}XX$, MS^2 *m/z* 845. Product ions named according to Domon and Costello (1988).

HILIC-MS and HILIC-MS/MS under optimized conditions. An HILIC-MS/MS method was created for each size of oligosaccharide. The MS^2 spectra of HILIC-MS/MS (Fig. 6) and direct infusion MS/MS were compared to each other. Some differences in fragmentation pattern and ion intensity were found. This might be due to the different pH of the eluent in HILIC-MS/MS and direct infusion. HILIC-MS/MS was run at pH 10 (to prevent anomeric peaks from splitting) and directly infused ESI-MS^n was run at pH 5.

All samples were found to form a specific MS^2 spectrum, although the spectra of XA^2XX (Fig. 6k) and X_5 (Fig. 6c) had very similar ion distributions. It was noticed that trisaccharides and tetrasaccharides can be identified by their base peaks (table of diagnostic peaks in OR 3). X_3 had *m/z* 263 (Fig. 6a), A^2X had *m/z* 335 (Fig. 6d)), and A^3X had *m/z* 281 (Fig. 6e). X_4 had *m/z* 395 (Fig. 6b), $D^{2,3}X$ had *m/z* 413 (Fig. 6f), $A^{2+3}X$ had *m/z* 467 (Fig. 6g), and A^2XX had *m/z* 395 (Fig. 6h) as their base peaks in the MS^2 spectrum. Even though A^2XX had the same base peak as X_4, it was easily differentiated from X_4 by the peak at *m/z* 335. Pentasaccharides had only base peaks at *m/z* 599 or *m/z* 617. Therefore, the presence or absence of other peaks was needed to define them. X_5 had *m/z* 281, *m/z* 467, *m/z* 599, and *m/z* 617 peaks (Fig. 6c). $A^{2+3}XX$ had *m/z* 263, *m/z* 467, and *m/z* 599 peaks (Fig. 6i). XA^3XX had *m/z* 263, *m/z* 299, *m/z* 599, and *m/z* 617 peaks (Fig. 6j). XA^2XX had *m/z* 467, *m/z* 599, and *m/z* 617 peaks (Fig. 6k). The following retention times were observed in HILIC in the current study: A^3X 10.3 min, A^2X 12.1 min, $A^{2+3}X$ 13.5 min, X_3 15.3 min, $D^{2,3}X$ 15.9 min, A^2XX 17.6 min, $A^{2+3}XX$ 18.5 min, X_4 20.7 min, XA^3XX 21.3 min, XA^2XX 22.4 min, $XA^{2+3}XX$ 24.3 min, and X_5 25.6 min. It was noted that the *O*-3-Ara*f*-substituted samples eluted before the *O*-2-Ara*f*-substituted samples and the di-substituted samples were last in the order. Samples with two Xyl*p* residue backbones eluted in the order of X_2, A^3X, A^2X, and $A^{2+3}X$, and samples with three Xyl*p* residue backbones in the order of X_3, A^2XX, and $A^{2+3}XX$. The elution order of four Xyl*p* residue backbone samples was X_4, XA^3XX, XA^2XX, and $XA^{2+3}XX$. In addition, the lengthening of the Xyl*p* backbone was found to increase the retention, and Ara*f* substitution decreased the retention, since the A^3X, A^2X, and $A^{2+3}X$ samples eluted faster than the linear X_3. Furthermore, the retention times were all different, which will confirm their identification in future studies.

4. Conclusions

The feasibility of negative ionization direct infusion ESI-MS^n and HILIC-MS/MS to analyze and identify the structures of cereal-derived (A)XOS was studied. Initially, the influence of linkage positions on fragmentation of (A)XOS was examined. It was found that negative ionization ESI-MS^n can characterize each linkage of linear (A)XOS. Each linkage produced diagnostic cross-ring fragments, the presence or absence of which can determine the linkage positions in (A)XOS. The (1 → 4)–linked Xyl*p* backbone produces $^{0,2}A$- and $^{0,2}A$-H_2O-ions. The (1 → 2)-linked residues produce $^{0,2}X_2$-ions from both Xyl*p* and Ara*f* residues. The (1 → 3)-linked residues lack the cross-ring fragment ions, except for the (1 → 3)-linked C_2-ion of A^3X. Also, the branched samples were found to fragment next to the branched residue by double glycosidic bond cleavages. The branched samples were determined by the presence or absence of diagnostic ions in the MS^3 spectra. It was also found that diagnostic ions (*m/z* 245 or *m/z* 299) in MS^3 can distinguish the studied branched samples from linear samples. Ion *m/z* 299 is also a diagnostic ion of *O*-3 and *O*-4 branched residues. Subsequently, HILIC-MS/MS was implemented for the identification of (A)XOS. The results

showed that the negative ionization HILIC-MS/MS method was efficient for identification of (A)XOS samples by using a now formed spectral library and chromatographic retention times. The implemented method will be most useful for the structural analysis and profiling of AX and mixtures of (A)XOS from different plant materials. If the AXOS sample has many branching points, the method can be improved with ^{18}O-labeling of the reducing end or separation with ion mobility mass spectrometry.

Acknowledgements

Financial support from the Raisio Plc Research Foundation is gratefully acknowledged.

Conflict of interest

The authors declare that they have no conflicts of interest regarding this work.

Appendix A. Supplementary data

Supplementary data to this article can be found online at https://doi.org/10.1016/j.foodchem.2018.09.074.

References

Asam, M. R., & Glish, G. L. (1997). Tandem mass spectrometry of alkali cationized polysaccharides in a quadrupole ion trap. *Journal of the American Society for Mass Spectrometry, 8*(9), 987–995.

Biliaderis, C., & Izydorczyk, M. (2007). Arabinoxylans: Technologically and nutritionally functional plant polysaccharides. In C. Biliaderis, & M. Izydorczyk (Eds.). *Functional food carbohydrates* (pp. 249–290). USA: CRC Press.

Bowman, M. J., Dien, B. S., Vermillion, K. E., & Mertens, J. A. (2014). Structural characterization of (1→2)-β-xylose-(1→3)-α-arabinose-containing oligosaccharide products of extracted switchgrass (Panicum virgatum, L.) xylan after exhaustive enzymatic treatment with α-arabinofuranosidase and β-endo-xylanase. *Carbohydrate Research, 398*, 63–71.

Broekaert, W. F., Courtin, C. M., Verbeke, K., Wiele, Van d., Verstraete, W., & Delcour, J. A. (2011). Prebiotic and other health-related effects of cereal-derived arabinoxylans, arabinoxylan-oligosaccharides, and xylooligosaccharides. *Critical Reviews in Food Science and Nutrition, 51*(2), 178–194.

Brokl, M., Hernández-Hernández, O., Soria, A. C., & Sanz, M. L. (2011). Evaluation of different operation modes of high performance liquid chromatography for the analysis of complex mixtures of neutral oligosaccharides. *Journal of Chromatography A, 1218*(42), 7697–7703.

Carroll, J. A., Willard, M. D., & Lebrilla, C. B. (1995). Energetics of cross-ring cleavages and their relevance to the linkage determination of oligosaccharides. *Analytica Chimica Acta, 307*(2), 431–447.

Chai, W., Piskarev, V., & Lawson, A. M. (2001). Negative-ion electrospray mass spectrometry of neutral underivatized oligosaccharides. *Analytical Chemistry, 73*(3), 651–657.

Chai, W., Lawson, A. M., & Piskarev, V. (2002). Branching pattern and sequence analysis of underivatized oligosaccharides by combined MS/MS of singly and doubly charged molecular ions in negative-ion electrospray mass spectrometry. *Journal of the American Society for Mass Spectrometry, 13*(6), 670–679.

Ciucanu, I. (2006). Per-O-methylation reaction for structural analysis of carbohydrates by mass spectrometry. *Analytica Chimica Acta, 576*(2), 147–155.

Domon, B., & Costello, C. E. (1988). A systematic nomenclature for carbohydrate fragmentations in FAB-MS/MS spectra of glycoconjugates. *Glycoconjugate Journal, 5*(4), 397–409.

Duus, J. O., Gotfredsen, C. H., & Bock, K. (2000). Carbohydrate structural determination by NMR spectroscopy: Modern methods and limitations. *Chemical Reviews, 100*(12), 4589–4614.

Everest-Dass, A., Kolarich, D., Campbell, M., & Packer, N. (2013). Tandem mass spectra of glycan substructures enable the multistage mass spectrometric identification of determinants on oligosaccharides. *Rapid Communications in Mass Spectrometry, 27*(9), 931–939.

Fauré, R., Courtin, C. M., Delcour, J. A., Dumon, C., Faulds, C. B., Fincher, G. B., Fort, S., Fry, S. C., Halila, S., Kabel, M. A., Pouvreau, L., Quemener, B., Rivet, A., Saulnier, L., Schols, H. A., Driquez, H., & O'Donohue, M. J. (2009). A brief and informationally rich naming system for oligosaccharide motifs of heteroxylans found in plant cell walls. *Australian Journal of Chemistry, 62*, 533–537.

Guan, B., & Cole, R. B. (2008). MALDI Linear-field reflectron TOF post-source decay analysis of underivatized oligosaccharides: Determination of glycosidic linkages and anomeric configurations using anion attachment. *Journal of the American Society for Mass Spectrometry, 19*(8), 1119–1131.

Harvey, D. (2005). Fragmentation of negative ions from carbohydrates: Part 1. Use of nitrate and other anionic adducts for the production of negative ion electrospray spectra from N-linked carbohydrates. *Journal of the American Society for Mass Spectrometry, 16*(5), 622–630.

Hernandez-Hernandez, O., Calvillo, I., Lebron-Aguilar, R., Moreno, F. J., & Sanz, M. L. (2012). Hydrophilic interaction liquid chromatography coupled to mass spectrometry for the characterization of prebiotic galactooligosaccharides. *Journal of Chromatography A, 1220*, 57–67.

Hofmeister, G. E., Zhou, Z., & Leary, J. A. (1991). Linkage position determination in lithium-cationized disaccharides: Tandem mass spectrometry and semiempirical calculations. *Journal of the American Chemical Society, 113*(16), 5964–5970.

Izydorczyk, M. S., & Biliaderis, C. G. (1995). Cereal arabinoxylans: Advances in structure and physiochemical properties. *Carbohydrate Polymers, 28*(1), 33–48.

Juvonen, M. (2011). Tandemmassaspektrometrinen menetelmä neutraalien isomeeristen oligosakkaridien rakenteen määrittämisessä (The structural analysis of neutral isomeric oligosaccharides by tandem mass spectrometry). EKT-Series, University of Helsinki, 1506. URN:NBN:fi:hulib-201507211856; http://hdl.handle.net/10138/28608.

Leijdekkers, A. G. M., Sanders, M. G., Schols, H. A., & Gruppen, H. (2011). Characterizing plant cell wall derived oligosaccharides using hydrophilic interaction chromatography with mass spectrometry detection. *Journal of Chromatography A, 1218*(51), 9227–9235.

Liu, J., Kisonen, V., Willför, S., Xu, C., & Vilaplana, F. (2016). Profiling the substitution pattern of xyloglucan derivatives by integrated enzymatic hydrolysis, hydrophilic-interaction liquid chromatography and mass spectrometry. *Journal of Chromatography A, 1463*(Supplement C), 110–120.

Maina, N. H., Juvonen, M., Domingues, R. M., Virkki, L., Jokela, J., & Tenkanen, M. (2013). Structural analysis of linear mixed-linkage glucooligosaccharides by tandem mass spectrometry. *Food Chemistry, 136*(3–4), 1496–1507.

Maslen, S. L., Goubet, F., Adam, A., Dupree, P., & Stephens, E. (2007). Structure elucidation of arabinoxylan isomers by normal phase HPLC-MALDI-TOF/TOF-MS/MS. *Carbohydrate Research, 342*(5), 724–735.

Matamoros Fernández, L. E., Obel, N., Scheller, H. V., & Roepstorff, P. (2003). Characaterization of plant oligosaccharides by matrix-assisted laser desorption/ionization and electrospray mass spectrometry. *Journal of Mass Spectrometry, 38*(4), 427–437.

Mendis, M., & Simsek, S. (2014). Arabinoxylans and human health. *Food Hydrocolloids*, 42. *Part, 2*, 239–243.

Mischnick, P. (2011). Mass spectrometric characterization of oligo- and polysaccharides and their derivatives. In M. Hakkarainen (Ed.). *Mass spectrometry of polymers – new techniques. Advances in polymer science* (pp. 105–174). Berlin, Heidelberg: Springer vol. 248.

Pastell, H., Virkki, L., Harju, E., Tuomainen, P., & Tenkanen, M. (2009). Presence of 1→3-linked 2-O-β-D-xylopyranosyl-α-L-arabinofuranosyl side chains in cereal arabinoxylans. *Carbohydrate Research, 344*(18), 2480–2488.

Pastell, H., Tuomainen, P., Virkki, L., & Tenkanen, M. (2008). Step-wise enzymatic preparation and structural characterization of singly and doubly substituted arabinoxylo-oligosaccharides with non-reducing end terminal branches. *Carbohydrate Research, 343*(18), 3049–3057.

Pfenninger, A., Karas, M., Finke, B., & Stahl, B. (2002a). Structural analysis of underivatized neutral human milk oligosaccharides in the negative ion mode by nano-electrospray MS n (Part 1: Methodology). *Journal of the American Society for Mass Spectrometry, 13*(11), 1331–1340.

Pfenninger, A., Karas, M., Finke, B., & Stahl, B. (2002b). Structural analysis of underivatized neutral human milk oligosaccharides in the negative ion mode by nano-electrospray MSn (part 2: Application to isomeric mixtures). *Journal of the American Society for Mass Spectrometry, 13*(11), 1341–1348.

Pollet, A., Delcour, J. A., & Courtin, C. M. (2010). Structural determinants of the substrate specificities of xylanases from different glycoside hydrolase families. *Critical Reviews in Biotechnology, 30*(3), 176–191.

Pu, J., Zhao, X., Xiao, L., & Zhao, H. (2017). Development and validation of a HILIC-ELSD method for simultaneous analysis of non-substituted and acetylated xylo-oligosaccharides. *Journal of Pharmaceutical and Biomedical Analysis, 139*, 232–237.

Quemener, B., Ordaz-Ortiz, J. J., & Saulnier, L. (2006). Structural characterization of underivatized arabino-xylo-oligosaccharides by negative-ion electrospray mass spectrometry. *Carbohydrate Research, 341*(11), 1834–1847.

Rantanen, H., Virkki, L., Tuomainen, P., Kabel, M., Schols, H., & Tenkanen, M. (2007). Preparation of arabinoxylobiose from rye xylan using family 10 *Aspergillus aculeatus* endo-1,4-β-D-xylanase. *Carbohydrate Polymers, 68*(2), 350–359.

Saulnier, L., Guillon, F., Sado, P., & Rouau, X. (2007). 2.20 – Plant cell wall polysaccharides in storage organs: Xylans (food applications). In H. Kamerling (Ed.). *Comprehensive Glycoscience* (pp. 653–689). Oxford: Elsevier.

Saulnier, L., Sado, P., Branlard, G., Charmet, G., & Guillon, F. (2007). Wheat arabinoxylans: Exploiting variation in amount and composition to develop enhanced varieties. *Journal of Cereal Science, 46*(3), 261–281.

Spina, E., Sturiale, L., Romeo, D., Impallomeni, G., Garozzo, D., Waidelich, D., & Glueckmann, M. (2004). New fragmentation mechanisms in matrix-assisted laser desorption/ionization time-of-flight/time-of-flight tandem mass spectrometry of carbohydrates. *Rapid Communications in Mass Spectrometry, 18*(4), 392–398.

Suzuki, S. (2013). Recent developments in liquid chromatography and capillary electrophoresis for the analysis of glycoprotein glycans. *Analytical Sciences, 29*(12), 1117–1128.

Wang, J., Yuan, X., Sun, B., Cao, Y., Tian, Y., & Wang, C. (2009). On-line separation and structural characterisation of feruloylated oligosaccharides from wheat bran using HPLC-ESI-MS n. *Food Chemistry, 115*(4), 1529–1541.

Zhu, J. H., & Cole, R. (2001). Ranking of gas-phase acidities and chloride affinities of monosaccharides and linkage specificity in collision-induced decompositions of negative ion electrospray-generated chloride adducts of oligosaccharides. *Journal of the American Society for Mass Spectrometry, 12*(11), 1193–1204.